International Journal of Control, Automation and Systems 17(X) (2019) 1-9
http://dx.doi.org/10.1007/s12555-018-0710-9
ISSN:1598-6446 eISSN:2005-4092
http://www.springer.com/12555

Quadrotor Flight Controller Design Using Classical Tools

Tomasz Zubowicz*, Krzysztof Arminski, and Arkadiusz Kusalewicz

Abstract: A principal aspect of quadrocopter in-flight operation is to maintain the required attitude of the craft's frame, which is done either automatically in the so-called supervised flight mode or manually during man-operated flight mode. This paper deals with the problem of flight controller (logical) structure and algorithm design dedicated for the man-operated flight mode. The role of the controller is to stabilise the rotational speeds of the Tait-Bryan angles. This work aims to extend the sustainable performance operating range of a proportional-integral-derivative output feedback compensator (PID) based flight controller by exploiting the concepts of feedforward inverse actuator model and the re-definition of input space in order to handle the non-linearity of the system under control. The proposed solution is verified numerically and implemented in the form of a discrete-time domain algorithm, obtained by emulation, using a physical quadrocopter model.

Keywords: Attitude control, drone, inverse model, PID.

1. INTRODUCTION

In recent years, man-operated Unmanned Aerial Vehicles (UAVs) have become a tool for the modern industry, commerce and a growing number of 'scale' modellers and the so-called do-it-yourself (DIY) projects with a lot of modelling community support.

In principal, the quadrocopter flight controller synthesis is a non-trivial task due to non-linear plant dynamics and its structural instability [1]. These features make mathematical modelling an important step frequently utilised to propose a control system design solution. A variety of models and control schemes have been proposed and documented in literature. In general, the available models differ in the level of complexity especially in the context of including an actuator (AC) system model (e.g., tilting propellers [2] or a power-source voltage drop [3]) and incorporation of the aerodynamic effects e.g., [4]. The control solutions proposed in literature to attitude control problem range from applications of 'classical' proportional-integral-derivative output feedback compensator (PID) controllers through non-linear and optimal control synthesis up to algorithms designed using model-based predictive control (MPC) approach. A PID attitude controller design with simulation based tuning has been proposed in [5]. An approach using optimised PID controller can be found in [6]. In [7] a cascade of PIDs has been utilised with Kalman filtration in feedback loops. In [8] a comparison of PID based control and linear–quadratic (LQ) approach has been presented. A fuzzy PID approach has been applied in [9]. In recent work [10] an optimised Fuzzy-Padé controller for attitude stabilisation of a quadrotor has been proposed. An adaptive sliding mode control design has been addressed in, e.g., [11, 12]. A self-tuning attitude and altitude control scheme has been derived in [13]. In [14] an H_∞ based feedback linearisation control scheme has been discussed. Lyapunov approach to control system design has been used in [15]. A robust (Lyapunov stable) proportional-derivative control with disturbance compensation has been addressed in [16]. The MPC based solutions have been addressed in [17,18]. Finally, a comprehensive review of available control solutions (up to year 2015) can be found in [19, 20].

Typically, off the shelf PID-based solutions suffer in performance from neglecting i.a. the non-linearity of the AC system. The goal of this work is to introduce an approach to the quadrocopter flight controller design based on the PID type controllers to enable stabilisation of the rotational speeds of the Tait-Bryan angles. To that goal, the quadrocopter flight controller is designed by applying a classical control theory utilising PID output feedback compensators and an inverse AC model in a feedforward loop. This has been done in order to cope with the AC system non-linearity and as such guaranteeing suit-

Manuscript received October 1, 2018; revised March 29, 2019; accepted July 30, 2019. Recommended by Associate Editor Seungkeun Kim under the direction of Editor Chan Gook Park. The research work was done under grant Polish MNiSW 8902/E-359/M/2017: Young Researcher Support Program. The authors wish to express their thanks for support.

Tomasz Zubowicz is with the Department of Electrical Engineering, Control Systems and Informatics, Faculty of Electrical and Control Engineering Gdańsk University of Technology, 80-233 Gdańsk, Poland (e-mail: tomasz.zubowicz@gmail.com). Krzysztof Arminski and Arkadiusz Kusalewicz are with Department Control Engineering, Faculty of Electrical and Control Engineering, Gdańsk University of Technology, 80-233 Gdańsk, Poland (e-mails: {krzysztof.arminski, arkadiuszkusalewicz}@gmail.com).
* Corresponding author.

able conditions for the core PID based algorithm. The proposed control design procedure is composed of two steps. First, based on previously obtained results [3, 21], the identified AC model is used in order to derive the inverse model which is subsequently applied to linearise the AC system. Second, the PIDs are tuned accordingly, utilising pole placement techniques, to meet the performance specifications. The physical model implementation algorithm is a discrete-time domain representation of the algorithm being designed. This is done by exploiting the emulation method by Tustin transform based on the Shannon-Kotelnikov sampling law.

The contribution of this paper is that it delivers a proposal of a solution which enables a sustainable performance of a PID based attitude controller over an increased (in comparison to direct application of PID e.g., [5]) range of operational states and conditions due to application of feedforward inverse AC model. The main drawback of the proposed solution resides with the uncertainty and nonlinearity leakage effects, caused by application of inverse model linearisation, assessment of which is a topic of current research work.

The paper is organised in the following manner: in Section 2 a problem formulation is given. Next, Section 3 models utilised for simulation and design are given. Then, Section 4 describes the key components of a proposed control system. The numerical results are given in Section 5. Section 6 provides the drawn conclusion.

2. PROBLEM FORMULATION

The control system main function is to control the on-flight behaviour of the quadrocopter by adjusting the desired thrust and rotational momentum in order to stabilise the rotational speeds with respect to the Tait-Bryan (pitch, roll and yaw) angles. To that goal the following assumptions originating from quadrocopter operating conditions and structural characteristics are formulated.

Assumption 1: Coordinates x, y and z are to be neglected in utility model structure.

Assumption 2: It is assumed that the model of AC system, comprised of the power system, motors and propellers is known (in terms of structure and parameters) and its internal dynamics are considered negligible.

The justification for Assumption 2 results from the following facts. First, the mass of the mechanical rotary parts is low in comparison to the mechanical inertia of the quadrocopter (QC) frame. Second, the time constants related to the electrical part of the AC system are shorter by at least one order of magnitude in comparison to the time constants of the inertia related to QC frame. This implies that the most of the effects observed due to acting AC system result from its static characteristics.

Assumption 3: The uncertainty caused by the difference of physical structure in between the four acting AC subsystems (motor and propeller pairs) is considered negligible.

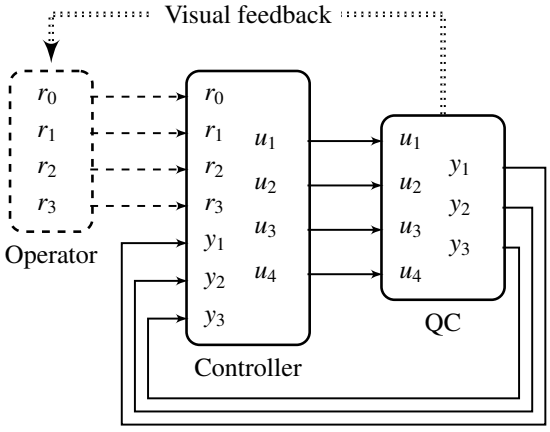

Fig. 1. Block diagram of a control system under design.

Assumption 4: It is assumed that the physical structure of quadrocopter is symmetric and its parameters are known.

Under the conditions given by Assumption 1-4 a general scheme of the closed loop (CL) control system has been proposed as depicted in Fig. 1. Set $\mathbb{R}$ is used to denote the real numbers and $\overline{(\cdot),(\cdot\cdot)}$ is used to denote an interval between $(\cdot)$ and $(\cdot\cdot)$ over the positive part of an integer field $\mathbb{Z}_+$, then: $\forall i \in \overline{1,3} : y_i \in \mathbb{R}$ are to denote the controlled variables, namely pitch, roll and yaw angular velocities, respectively. The control variables $u_i \in \mathbb{R}$, $\forall i \in \overline{1,4}$ are the pulse point modulated (PPM) times triggering the power system in order to deliver the required motor voltages to generate QC thrust and rotations in three dimensional space and in consequence desired movement. The role of an 'Operator' is to design a path of desired movement of the QC based on the visual information feedback of the current QC's position and movement in space. This information is then supplied to the controller in the form of four reference signals $r_i \in \mathbb{R}$, $\forall i \in \overline{0,3}$, namely the thrust, pitch, roll and yaw angular velocities. Based on the desired r_i, $\forall i \in \overline{0,3}$, and measurement feedback information y_i, $\forall i \in \overline{1,3}$ the 'Controller' generates appropriate control signals (u_i, $\forall i \in \overline{1,4}$). The signal line type in Fig. 1 is set up in order to distinguish in between the wired (solid line), wireless (dashed line) and visual/eye contact (dotted line) information feedback used within the system. The goal is to obtain a controller $\mathcal{R}$ acting as a map from the joint reference and measurement domain into the control signal domain as: $\mathcal{R} : \mathbb{R}^4 \times \mathbb{R}^3 \to \mathbb{R}^4$. It is clear that the dimensionality of the problem requires special treatment in order to be kept in the classical control output feedback framework. For that reason an internal structure of $\mathcal{R}$ is proposed as depicted in Fig. 2. The key features of the pro-

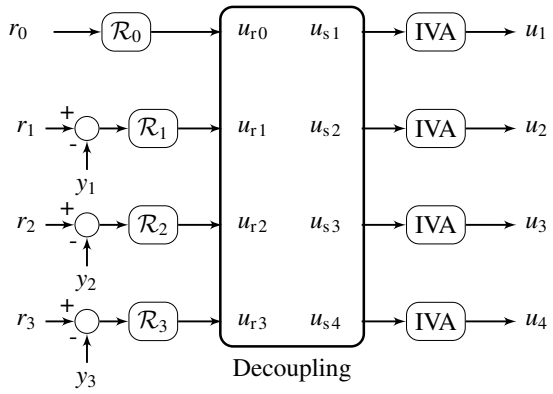

Fig. 2. Flight controller internal structure.

posed controller reside with inverse actuator model (IVA) of the control elements utilised in order to handle AC nonlinearity, to be addressed in terms of a signal transform $\mathcal{L}_{\text{IVA}}$, and the 'Decoupling' block that invokes the input space transform $\mathcal{L}_{\text{I}}$ (having also the decoupling properties) used to handle the dimensionality mismatch in between the control and controlled (using measurement feedback) variables. These internal controller mechanisms are addressed in detail in the following sections of the paper.

In consequence, the four internal acting controllers can be designed as of PID type, namely one open loop proportional type ($\mathcal{R}_0$) set up to handle thrust (r_0) and three PIDs ($\mathcal{R}_i$, $\forall i \in \overline{1,3}$) dedicated for pitch ($r_1$), roll ($r_2$) and yaw ($r_3$) rotational speeds, respectively. Notably, the thrust remains a controlled variable, though the 'feedback' information loop is 'closed' by an operator which is a reasonable solution to allow one to account for the vast uncertainty related to the surrounding environment without the necessity to deploy a complex (higher in control system hierarchy) supervisory layer (e.g., [22]). This also includes the information on the deviation of the thrust vector from the gravitational force vector. Hence, the true role of $\mathcal{R}_0$ is reduced to simple signal scaling. Therefore, technically it follows that $\mathcal{R}$:

$$(u_{\text{s}1}, u_{\text{s}2}, u_{\text{s}3}, u_{\text{s}4}) \stackrel{\text{def}}{=} (\mathcal{L}_{\text{IVA}} \circ \mathcal{L}_{\text{I}})\,(u_{\text{r}0}, u_{\text{r}1}, u_{\text{r}2}, u_{\text{r}3})\,, \tag{1}$$

where $u_{\text{r}0} \stackrel{\text{def}}{=} \mathcal{R}_0(r_0)$ and $u_{ri} \stackrel{\text{def}}{=} \mathcal{R}_i(e_i)$, $\forall i \in \overline{1,3}$, where $e_i \stackrel{\text{def}}{=} r_i - y_i$ denotes the ith output feedback controller related control error.

3. QUADROCOPTER MODELS

The conceptual internal structure of the QC has been illustrated in Fig. 3. The QC, in principal, is composed of the main body ('QC body') and four motor–blade pairs ('S') connected to a power supply system ('Z') acting altogether as the AC system.

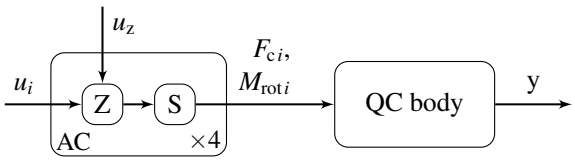

Fig. 3. QC block diagram.

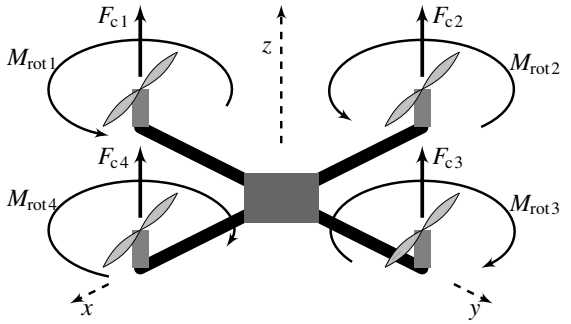

Fig. 4. Conceptual QC structure.

3.1. Quadrocopter body model for simulation purposes

Applying the Newton-Euler equations of motion to describe the QC mechanics in three dimensional space (Fig. 4) yields a simulation model $\mathcal{M}_{\text{p}}$.
The structure of the $\mathcal{M}_{\text{p}}$ is given by:

$$\ddot{\alpha}_{\text{x}} = \dot{\alpha}_{\text{y}}\dot{\alpha}_{\text{z}}\frac{I_{\text{xy}} - I_{\text{z}}}{I_{\text{xy}}} + \frac{l}{I_{\text{xy}}}\left(-F_{\text{c}2} + F_{\text{c}4}\right), \tag{2a}$$

$$\ddot{\alpha}_{\text{y}} = \dot{\alpha}_{\text{x}}\dot{\alpha}_{\text{z}}\frac{I_{\text{z}} - I_{\text{xy}}}{I_{\text{xy}}} + \frac{l}{I_{\text{xy}}}\left(F_{\text{c}1} - F_{\text{c}3}\right), \tag{2b}$$

$$\ddot{\alpha}_{\text{z}} = \frac{l}{I_{\text{z}}}\sum_{i=1}^{4}(-1)^i M_{\text{rot}\,i}. \tag{2c}$$

where x, y, z denote the QC's coordinate frame in three dimensional space; $\alpha_{\text{x}}, \alpha_{\text{y}}, \alpha_{\text{z}} \in \mathbb{R}$ are the Tait-Bryan (yaw, pitch and roll) angles; $I_{i_{\text{idx}}}, \forall i_{\text{idx}} \in \{\text{'x'}, \text{'y'}, \text{'z'}\}$, denote the moment of inertia with respect to the basis of QC's coordinate frame. In order for the utility model to be well-defined it is crucial to identify the parameters of the derived structure, namely: $p_{\text{d}} \stackrel{\text{def}}{=} [I_{\text{xy}}, I_{\text{z}}, l]^T$ as well as the shape and parameter of the *functions* $F_{\text{c}i} \stackrel{\text{def}}{=} F_{\text{c}i}(u_i, u_{\text{z}})$ and $M_{\text{rot}\,i} \stackrel{\text{def}}{=} M_{\text{rot}\,i}(u_i, u_{\text{z}})$, $\forall i$, e.g., [3, 21].

Assumption 4 implies that the moment of inertia along x and y axes coincide, thus: $I_{\text{x}} \stackrel{\text{def}}{=} I_{\text{xy}}$ and $I_{\text{y}} \stackrel{\text{def}}{=} I_{\text{xy}}$.

Finally, model (2) is utilised in simulation in order to predict the behaviour of the quadrocopter.

3.2. Quadrocopter body model for control design purposes

Since the flight controller is to stabilise the angular velocities by applying linear control laws therefore defining an operating point: $P_{\text{op}} = (\omega_{\text{x}},\ \omega_{\text{y}},\ \omega_{\text{z}},\ F_1,\ F_2,\ F_3,\ F_4,\ M_{\text{rot}\,1},$

$M_{\mathrm{rot}2}$, $M_{\mathrm{rot}3}$, $M_{\mathrm{rot}4})|_{\mathrm{op}}$ and finding a linear approximation $\mathcal{M}_{\mathrm{u}}$ (by utilising Taylor series expansion) of (2) is considered prudent and yields:

$$\mathcal{M}_{\mathrm{u}}: \begin{cases} \dot{\omega}_{\mathrm{x}} = \dfrac{L}{I_{\mathrm{x}}}(F_{\mathrm{c}3} - F_{\mathrm{c}1}), \\ \dot{\omega}_{\mathrm{y}} = \dfrac{L}{I_{\mathrm{x}}}(F_{\mathrm{c}4} - F_{\mathrm{c}2}), \\ \dot{\omega}_{\mathrm{z}} = \dfrac{1}{I_{\mathrm{x}}}\left(-M_{\mathrm{rot}1} + M_{\mathrm{rot}2} - M_{\mathrm{rot}3} + M_{\mathrm{rot}4}\right), \end{cases} \tag{3}$$

where $\omega_{(\cdot)} \overset{\mathrm{def}}{=} \dot{\alpha}_{(\cdot)}$ and is introduced only to increase intuitive perception of the problems addressed in the following sections.

It is worth to notice that the information on the cross couplings in the model dynamics is now lost. This affects the controller performance as shown in Section 5.

3.3. Actuator model

The AC system model is defined as a map $\mathbb{R}^4_+ \to \mathbb{R}^8_+$ of four identical (please recall Assumption 3) disjoint mappings $\mathbb{R}^1_+ \to \mathbb{R}^2_+$ given $\forall i \in \overline{1,4}$ as:

$$f_{\mathrm{AF}}: \quad F_{\mathrm{c}i}(u_i, u_{\mathrm{z}}) = f_{\mathrm{A}}(u_i; \theta_{\mathrm{a}}(u_{\mathrm{z}}), \theta_{\mathrm{c}}), \tag{4a}$$

$$f_{\mathrm{AM}}: \quad M_{\mathrm{rot}i}(u_i, u_{\mathrm{z}}) = f_{\mathrm{A}}(u_i; \theta_{\mathrm{b}}(u_{\mathrm{z}}), \theta_{\mathrm{c}}). \tag{4b}$$

where by taking $\theta_{\mathrm{a}} \overset{\mathrm{def}}{=} \theta_{\mathrm{a}}(u_{\mathrm{z}})$ and $\theta_{\mathrm{b}} \overset{\mathrm{def}}{=} \theta_{\mathrm{b}}(u_{\mathrm{z}})$ it follows that: $f_{\mathrm{A}}(u_i; \theta_{\mathrm{a}}, \theta_{\mathrm{c}}) \overset{\mathrm{def}}{=} \theta_{\mathrm{a}}(u_i - \theta_{\mathrm{c}})^2$ defines the AC subsystem model structure which acts from $\mathbb{R}_+$ to $\mathbb{R}_+$ and depends $\forall u_{\mathrm{z}}$ on $\theta_{\mathrm{a}}, \theta_{\mathrm{c}} \in \mathbb{R}$; θ_{c} is the time translation factor of PPM which is obtained directly from the hardware parameters. It should be noted that θ_{a}, θ_{b} are identified from the laboratory measurement data and are known to be dependent in general on the battery voltage level u_{z} as it has been shown in [3, 21], and $u_i \overset{\mathrm{def}}{=} \mathrm{sat}_{u_{\max}}(u_{\mathrm{s}i})$ where $u_{\max}$ is the max PPM time and:

$$\mathrm{sat}_{(\cdot\cdot)}(\cdot) \overset{\mathrm{def}}{=} \begin{cases} -(\cdot\cdot), & \text{if } (\cdot) \in (-\infty, (\cdot\cdot)), \\ (\cdot), & \text{if } (\cdot) \in [-(\cdot\cdot), (\cdot\cdot)], \\ (\cdot\cdot), & \text{if } (\cdot) \in ((\cdot\cdot), \infty). \end{cases} \tag{5}$$

Inserting (4) to either (2) or (3) results in obtaining the QC simulation model or the model used for flight controller design purposes (resembling the structure as depicted in Fig. 3).

4. CONTROL SYSTEM DESIGN

The control system design task is considered in this section by addressing the consecutive controller subsystems as depicted in Fig. 2.

4.1. Inverse actuator model design

The inverse input space transform $\mathcal{L}_{\mathrm{IVA}}$ is defined as:

$$\mathcal{L}_{\mathrm{IVA}}: f^{-1}_{\mathrm{AF}}\left(u_{\mathrm{s}i}, \tilde{\theta}_{\mathrm{a}}, \theta_{\mathrm{c}}\right) \overset{\mathrm{def}}{=} \sqrt{\frac{1}{\tilde{\theta}_{\mathrm{a}}} u_{\mathrm{s}i}} + \theta_{\mathrm{c}}, \tag{6}$$

where $\tilde{\theta}_{\mathrm{a}}$ represents the best available knowledge (mean value) on θ_{a}. As a consequence, it follows that under $\mathcal{L}_{\mathrm{IVA}}$ the transformation of (4a) is exact if $\tilde{\theta}_{\mathrm{a}} = \theta_{\mathrm{a}}$ and yields:

$$\mathcal{L}_{\mathrm{IVA}} \circ f_{\mathrm{AF}} \equiv 1, \tag{7}$$

while applied to (4b) looses this property and for $\tilde{\theta}_{\mathrm{b}} = \theta_b$ it occurs that:

$$\mathcal{L}_{\mathrm{IVA}} \circ f_{\mathrm{AM}} \equiv \frac{\tilde{\theta}_{\mathrm{b}}}{\tilde{\theta}_{\mathrm{a}}}, \tag{8}$$

where $\tilde{\theta}_{\mathrm{b}}$ has an analogous interpretation as $\tilde{\theta}_{\mathrm{a}}$.

In consequence, the non-linearity caused by AC is compensated only when considering perfect knowledge on the AC model and is only mitigated otherwise. Therefore, (3)-(4) are rewritten using (6) as:

$$\mathcal{M}_{\mathrm{uIVA}}: \begin{cases} \dot{\omega}_{\mathrm{x}} = \dfrac{L}{I_{\mathrm{x}}}(u_{\mathrm{s}3} - u_{\mathrm{s}1}), \\ \dot{\omega}_{\mathrm{y}} = \dfrac{L}{I_{\mathrm{x}}}(u_{\mathrm{s}4} - u_{\mathrm{s}2}), \\ \dot{\omega}_{\mathrm{z}} = \dfrac{1}{I_{\mathrm{x}}}\dfrac{\tilde{\theta}_{\mathrm{b}}}{\tilde{\theta}_{\mathrm{a}}}(-u_{\mathrm{s}1} + u_{\mathrm{s}2} - u_{\mathrm{s}3} + u_{\mathrm{s}4}). \end{cases} \tag{9}$$

The resulting $\mathcal{M}_{\mathrm{uIVA}}$ is to undergo input space transformation in order to proceed with a PID controller synthesis.

4.2. Inputs decoupling

In order to exert a control under skew dimensionality in control inputs and controlled outputs an input space transformation is applied as:

$$\mathcal{L}_{\mathrm{I}}: \begin{bmatrix} u_{\mathrm{s}1} \\ u_{\mathrm{s}2} \\ u_{\mathrm{s}3} \\ u_{\mathrm{s}4} \end{bmatrix} = \mathbb{G} \begin{bmatrix} u_{\mathrm{r}1} \\ u_{\mathrm{r}2} \\ u_{\mathrm{r}3} \end{bmatrix} + \mathbb{H} u_{\mathrm{r}0}, \tag{10}$$

where

$$\mathbb{G} = \begin{bmatrix} 0 & 1 & -1 \\ -1 & 0 & 1 \\ 0 & -1 & -1 \\ 1 & 0 & 1 \end{bmatrix}, \quad \mathbb{H} = \begin{bmatrix} 1 \\ 1 \\ 1 \\ 1 \end{bmatrix}. \tag{11}$$

Inserting (10) into (9) results in:

$$\mathcal{M}_{\mathrm{uIVAI}}: \begin{cases} \dot{\omega}_{\mathrm{x}} = 2\dfrac{l}{I_{\mathrm{x}}} u_{\mathrm{r}1}, \\ \dot{\omega}_{\mathrm{y}} = 2\dfrac{l}{I_{\mathrm{y}}} u_{\mathrm{r}2}, \\ \dot{\omega}_{\mathrm{z}} = 4\dfrac{1}{I_{\mathrm{z}}}\dfrac{\tilde{\theta}_{\mathrm{b}}}{\tilde{\theta}_{\mathrm{a}}} u_{r3}, \end{cases} \tag{12}$$

which is utilised to design controllers $\mathcal{R}_i$, $\forall i \in \overline{1,3}$. Notably, $\mathcal{M}_{\text{uIVAI}}$ due to its structure can in fact be handled as a set of three linear, mutually independent, systems.

4.3. Controller synthesis

Taking (12) and defining $\boldsymbol{G}(s)$ to be a transfer function in s-domain (under zero initial conditions) acting from the controller output space to angular velocity space yields:

$$\begin{aligned}\boldsymbol{G}(s) &\overset{\text{def}}{=} \operatorname{diag}\{G_1(s), G_2(s), G_3(s)\} \\ &= \operatorname{diag}\left\{2\frac{l}{I_\text{x}}\frac{1}{s}, 2\frac{l}{I_\text{y}}\frac{1}{s}, 4\frac{1}{I_\text{z}}\frac{\tilde{\theta}_\text{b}}{\tilde{\theta}_\text{a}}\frac{1}{s}\right\}. \end{aligned} \tag{13}$$

Under Assumption 3 and 4 it can be found that:

$$G_1(s) \equiv G_2(s) \equiv G_{12}(s) \equiv 2\frac{l}{sI_\text{xy}}. \tag{14}$$

It follows that under the physical interpretation of r_i, $\forall i \in \overline{1,3}$ and noisy sensor information the following PID structure is proposed:

$$\forall i \in \overline{1,3}, \mathcal{R}_i : \begin{cases} u_{\text{p}i}(t) = k_{\text{p}i}e_i(t) + k_{\text{I}i}\int_0^t u_{\text{Ip}i}(\tau)d\tau, \\ u_{\text{r}i}(t) = sat_{(u_{i\max})}(u_{\text{p}i}(t)), \end{cases} \tag{15}$$

where $\forall i$, $k_{\text{p}i}$, $k_{\text{I}i} > 0$ (for stability requirements at P_op), with:

$$u_{\text{Ip}i}(t) = \begin{cases} e_i(t), & \text{if } (u_{Ii}(t), e_i) \in \Omega_\text{AW}, \\ 0, & \text{otherwise}, \end{cases} \tag{16}$$

and

$$\begin{aligned}\Omega_\text{AW} \overset{\text{def}}{=} &(-u_{i\max}, u_{i\max}) \times \mathbb{R} \cup (-\infty, -u_{i\max}] \times (0, \infty) \\ &\cup [u_{i\max}, \infty) \times (-\infty, 0), \end{aligned} \tag{17}$$

which is then emulated into the discrete time-domain form implementation purposes using Tustin transform with respect to Shannon–Kotelnikov sampling law.

Assuming, for the sake of the design procedure, that the QC operates under normal operating conditions (the control is not saturated), the CL system description takes the form of:

$$G_1^\text{cl}(s) \equiv G_2^\text{cl}(s) = \frac{L_2(s)}{M_2(s)} = \frac{\theta_1 k_{\text{p}2}s + \theta_1 k_{\text{i}2}}{s^2 + \theta_1 k_{\text{p}2}s + \theta_1 k_{\text{i}2}}, \tag{18}$$

and

$$G_3^\text{cl}(s) = \frac{L_3(s)}{M_3(s)} = \frac{\theta_2 k_{\text{p}3}s + \theta_2 k_{\text{i}3}}{s^2 + \theta_2 k_{\text{p}3}s + \theta_2 k_{\text{i}3}}, \tag{19}$$

where $\theta_1 \overset{def}{=} 2\frac{lp}{I_\text{x}}$ and $\theta_2 \overset{def}{=} 4\frac{lp}{I_\text{z}}\frac{\tilde{\theta}_b}{\tilde{\theta}_a}$; and is utilised in order to place the poles at the desired location for the closed loop system to behave according to specification. Indeed, this can be done by considering the poles and zeros of the system. To that goal, a pole placement based on a method of pair of dominating poles (a reference to second order system dynamics) has been utilised. The drawback of this approach is that the anti-windup mechanisms are neglected at this step of the design procedure. The anti-windup strategy is added in the following step and verified in extensive numerical experiments to only grasp its impact on the closed loop system behaviour e.g., under finite set of representative disturbance scenarios considered. Deriving such a set of scenarios is a non-trivial task on its own and is not considered in this paper.

5. RESULTS

In this Section, first, the experiment conditions have been introduced (Subsection 5.1), followed by results and discussion (Subsection 5.2).

5.1. Experiment setup

Taking (2), (4) – (5) and the parameters $\tilde{\theta}_\text{a} = 7.3 \cdot 10^{-4}$ and $\tilde{\theta}_\text{b} = 8.7 \cdot 10^{-5}$ (acquired by considering a Chebyshev center of the bounded uncertainty model of an AC system identified according to [3]) produces the open-loop QC's simulation model.

The QC's operating point is selected as: $P_{op} = (0, 0, 0, F/4, F/4, F/4, F/4, M, M, M, M)$ and coincides with natural equilibrium point of open-loop QC dynamics in order to distribute the uncertainty caused by a linearisation error.

The control system performance requirements are given by percentage overshoot $P.O.$ which is assumed to be negligible to cope with the approximations made (e.g., Section 3.2) and the settling time (with 5% tolerance) $T_{settl\,5\%} \leq 1$ s. This, by the virtue of the second order system dynamics (e.g., [23]), translates into the following inequality: $\frac{3}{\Omega\zeta} \leq T_\text{settl}$, where Ω is the closed loop system natural frequency and ζ is the damping ratio, from which $\zeta = 1$ is selected as to ensure a possibly fast QC's response. From this it follows directly that $\Omega = 3$ so the desired closed loop dynamics is characterised by the following reference characteristic equation M_ref:

$$M_\text{ref}(s) = s^2 + 2\zeta\Omega s + \Omega^2. \tag{20}$$

Finally, the continuous time domain controller gains are obtained by a simple comparison of terms in between the $M_\text{ref}(s)$ and $M_{12}(s)$ and $M_3(s)$, respectively. The result of pole placement in terms of the PID gains (defined in (15)) are given in the first column ('Continuous Time-domain Gains (CTG)') of Table 1. Applying the design by emulation under Tustin transform and the known value of sampling time interval $T_\text{s} = 4 \cdot 10^{-3}$ s (obtained based on the QC bandwidth with respect to the Shannon-Kotelnikov sampling law) yields the 'Discrete

Table 1. Discrete-time PID controller parameters.

Controller	CTG		DTG		DTGT	
	k_p	k_i	K_p	K_i	K_p	K_i
$\mathcal{R}_1$	23,8	35,6	23,8	35,6	10.9	0.526
$\mathcal{R}_2$	23,8	35,6	23,8	35,6	10.9	0.526
$\mathcal{R}_3$	24,1	36,1	24,1	36,1	11.6	0.53

Time-domain controller Gains (DTG)' as given in the second column of Table 1. Including the simulation experiments results in the following final on-plant controller gains — 'Discrete Time-domain Gains - Tuned (DTGT)' column in Table 1. One should notice that the tuning was performed to move the closed-loop system poles in a manner guarantying increased damping (overshoot reduction).

5.2. Numerical validation

Experiments addressed in this section have been performed for two distinct power source voltage levels, namely nominal 12 V and lowered 11 V scenarios, in order to illustrate the behaviour of the control system mechanisms under typical operational conditions resulting from the effects of battery discharge. This is considered a viable approach since the discharge rate is negligible in comparison to the closed-loop QC's dynamics.

5.2.1 Inverse model

The test of the inverse model linearising mechanism $\mathcal{L}_{\mathrm{IVA}}$ was carried out as a comparison of the $u_{\mathrm{r}(\cdot)}$ with the forces acting on the QC body (frame). The results depicted in Fig. 5 illustrate that under considered experiment conditions the $u_{\mathrm{r}(\cdot)}$ signals do not always coincide with the forces acting on the QC body. The observed differences are caused by the signal windup. Analogous effects can be observed with respect to the angular momentum as depicted in Fig. 6. This verifies the effectiveness and limitations of the mechanism under the design conditions.

5.2.2 Decoupling

In Fig. 7 an illustration of the input space decoupling mechanism work-flow has been presented by simply showing that it is possible to carry out the control of QC dynamics in independent manner considering r_i, $\forall i$ (compare with Figs. 5-6 where the changes of inputs due to curse of experiment affect all signals).

5.2.3 Control system performance

The results of the experiments illustrating the proposed control system performance, for comparative reasons, have been put against the trajectories acquired by applying a 'classical' PID algorithms.

The attitude control system performance has been quantified using ℓ^1, ℓ^2 and ℓ^∞ norms in Table 2 and (qualitatively) depicted in Fig. 8. It can observed that the control

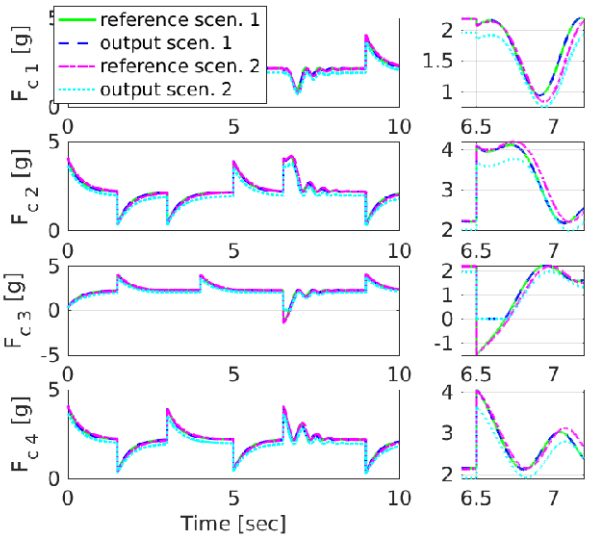

Fig. 5. Thrust forces and $u_{\mathrm{r}(\cdot)}$ trajectories.

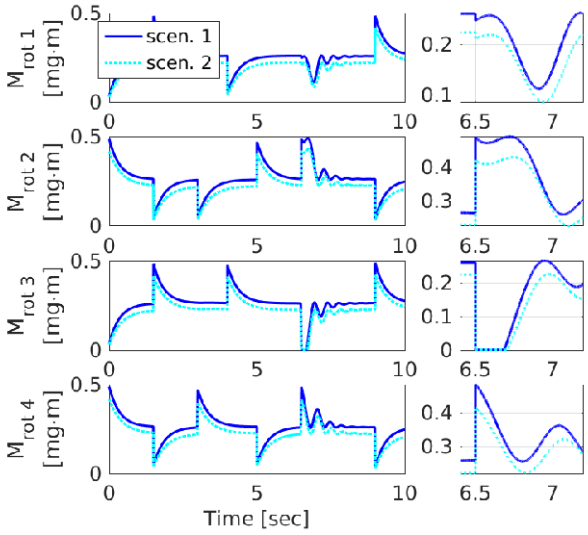

Fig. 6. Motor angular momentum trajectories.

system is able to stabilise a single controlled variable at a nonzero level. However, this generates an interaction (lost due to linearisation procedure) which distorts the physically coupled output variable. The corresponding control signals have been depicted in Fig. 9. At first it can be noticed that it promotes AC 'longevity' due to lack of extensively fast variations or signal hammering. The observed in Fig. 9 active AC system amplitude limitations are due to the $\mathcal{L}_{\mathrm{IVA}} \circ \mathcal{L}_{\mathrm{I}}$ transform of the two PID controllers outputs being highly active simultaneously. This indicates that the typical (used also in this research work) anti-windup scheme requires more insight in order to handle AC system limitations in a more suitable manner.

Notably, for the purpose of this experiment, the 'classi-

Table 2. Control error and control signal assessment.

Signal	e_1		e_2		e_3		u_1			u_2			u_3			u_4		
Norm	ℓ^1	ℓ^2	ℓ^1	ℓ^2	ℓ^1	ℓ^2	ℓ^1	ℓ^2	ℓ^∞	ℓ^1	ℓ^2	ℓ^∞	ℓ^1	ℓ^2	ℓ^∞	ℓ^1	ℓ^2	ℓ^∞
Scen 1	1.1	9.6	1.5	12	2.3	20	36	4.7e3	3.5e2	49	6.9e3	3.4e2	45	1.0e4	5.5e2	45	6.0e3	3.4e2
Scen 2	1.3	11	1.7	13	2.6	23	41	5.3e3	3.5e2	54	7.6e3	3.3e2	50	1.1e4	5.5e2	49	6.5e3	3.3e2
PID	1.1	9.8	1.7	13	2.4	20	35	4.1e3	2.3e2	48	6.4e3	2.5e2	40	5.7e3	2.4e2	44	5.0e3	2.4e2

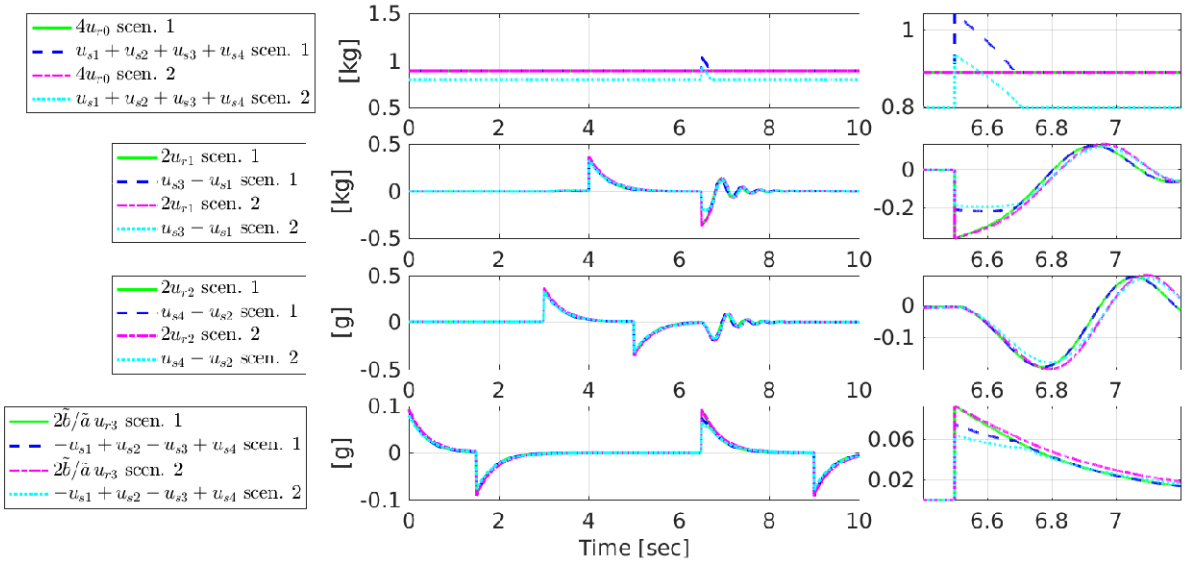

Fig. 7. Effects of the input decoupling.

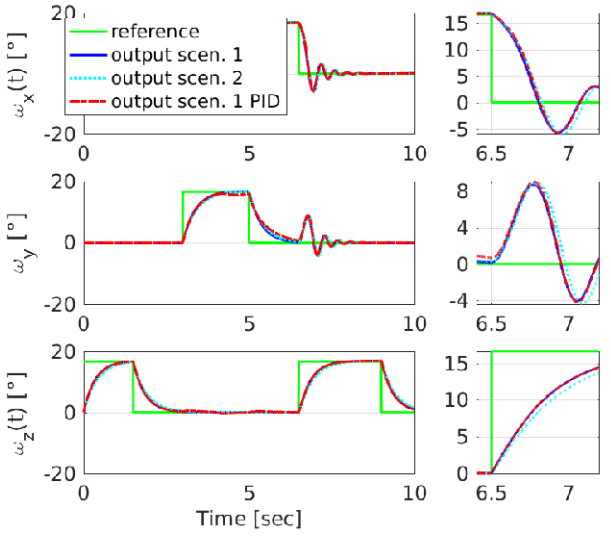

Fig. 8. Controlled output.

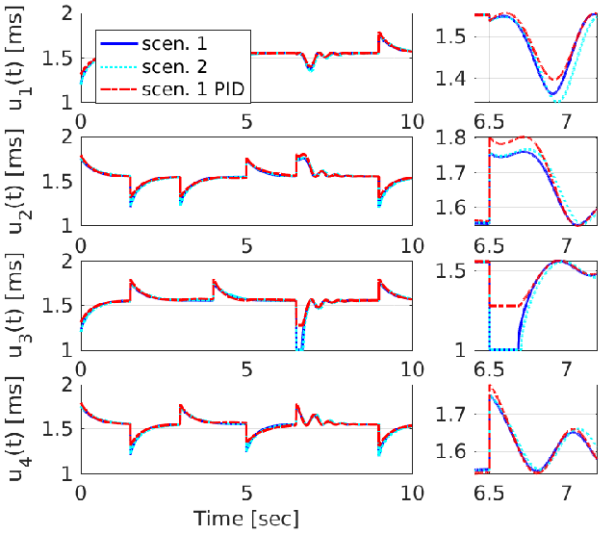

Fig. 9. Control signal.

cal' PID has been tuned using analogous performance requirements, as in the case of the proposed solution, using tangent approximation of the QC model non-linear term at P_{op} and consequently emulated into discrete-time format.

The project final results are that the constructed physical model of the QC is able to operate airborne under operators guidance. The on-boar 'black box' mechanisms are currently under design.

6. CONCLUSIONS

In this paper a modified (using inverse actuator model term) PID-based attitude controller design approach has been proposed. The input decoupling transformation was

applied to solve the problems related to the difference in the dimensionality of the control input and controlled variable spaces. This resulted in the overall non-linear controller which synthesis is based on classical approach by utilising well established PID output feedback controllers. The main advantage of the proposed solution is that it extends the QC's sustainable performance operating range. The results have been verified by simulations (including comparison to 'classical' PID) and deployed using testbed environment. The ongoing research aim is to include the on-board black-box for sensor data acquisition, ensure the robustness of the design, improve the anti-windup scheme and address the effects of the so-called non-linearity leakage caused by the applied inverse model transform.

REFERENCES

[1] G. Cai, B. M. Chen, and T. H. Lee, *Unmanned Rotorcraft Systems*, Springer Science & Business Media, 2011.

[2] M. Ryll, H. H. Bülthoff, and P. R. Giordano, "Modeling and control of a quadrotor UAV with tilting propellers," *Proc. of the IEEE International Conference on Robotics and Automation (ICRA)*, pp. 4606-4613, May 2012.

[3] K. Arminski and T. Zubowicz, "Robust identification of quadrocopter model for control purposes," *Proc. of the IEEE International Conference on Methods and Models in Automation and Robotics (MMAR)*, pp. 337-342, August 2017.

[4] G. Hoffmann, H. Huang, S. Waslander, and C. Tomlin, "Quadrotor Helicopter Flight Dynamics and Control: Theory and Experiment," *Proc. of the 2007-6461 AIAA Guidance, Navigation and Control Conference and Exhibit*, Jun 2007.

[5] J. Li and Y. Li, "Dynamic analysis and PID control for a quadrotor," *Proc. of the 2011 IEEE International Conference on Mechatronics and Automation*, pp. 573-578, August 2011.

[6] H. Bolandi, M. Rezaei, R. Mohsenipour, H. Nemati, and S. M. Smailzadeh, "Attitude Control of a Quadrotor with Optimized PID Controller," *Intelligent Control and Automation*, vol. 4, pp. 335-342, August 2013.

[7] Y. Wang, P. Li, Z. Lan, B. Li, and C. Li, "Quadrotor Aircraft Design based on the K60 Controller," *Journal of Engineering Science and Technology Review*, vol. 10, pp. 21-30, December 2017.

[8] S. Bouabdallah, A. Noth, and R. Siegwart, "PID vs LQ control techniques applied to an indoor micro quadrotor," *Proc. of the IEEE/RSJ International Conference on Intelligent Robots and Systems (IROS) (IEEE Cat. No.04CH37566)*, vol. 3, pp. 2451-2456, September 2004.

[9] C. Zhang, X. Zhou, H. Zhao, A. Dai, and H. Zhou, "Three-dimensional fuzzy control of mini quadrotor UAV trajectory tracking under impact of wind disturbance," *Proc. of the 2016 International Conference on Advanced Mechatronic Systems, ICAMechS*, pp. 372-377, November-December 2016.

[10] S. Salehfard, T. Abdollahi, C.-H. Xiong, and Y.-H. Ai, "An optimized Fuzzy-Padé controller applied to attitude stabilization of a quadrotor," *International Journal of Control, Automation and Systems*, vol. 16, pp. 1425-1434, June 2018.

[11] D. Lee, H. Jin Kim, and S. Sastry, "Feedback linearization vs. adaptive sliding mode control for a quadrotor helicopter," *International Journal of Control, Automation and Systems*, vol. 7, pp. 419-428, June 2009.

[12] Y. Yang and Y. Yan, "Attitude regulation for unmanned quadrotors using adaptive fuzzy gain-scheduling sliding mode control," *Aerospace Science and Technology*, vol. 54, pp. 208-217, July 2016.

[13] T. N. Dief, S. Yoshida, and M. Abdelhady, "Attitude and altitude stabilization of quad rotor using parameter estimation and self-tuning controller," *Proc. of the AIAA Atmospheric Flight Mechanics Conference*, June 2015.

[14] A. Mokhtari, A. Benallegue, and B. Daachi, "Robust feedback linearization and GH∞ controller for a quadrotor unmanned aerial vehicle," *Proc. of the IEEE/RSJ International Conference on Intelligent Robots and Systems, IROS*, vol. 57, pp. 1009-1014, September 2005.

[15] A. Tayebi and S. McGilvray, "Attitude stabilization of a VTOLvtol quadrotor aircraft," *IEEE Trans. on Control Systems Technology*, vol. 14, pp. 562-571, May 2006.

[16] A. P. Sandiwan, A. Cahyadi, and S. Herdjunanto, "Robust proportional-derivative control on SO(3) with disturbance compensation for quadrotor UAV," *International Journal of Control, Automation and Systems*, vol. 15, pp. 2329-2342, October 2017.

[17] A. Tzes, G. Nikolakopoulos, and K. Alexis, "Model predictive quadrotor control: attitude, altitude and position experimental studies," *IET Control Theory & Applications*, vol. 6, pp. 1812-1827, August 2012.

[18] A. Aswani, P. Bouffard, and C. Tomlin, "Extensions of learning-based model predictive control for real-time application to a quadrotor helicopter," *Proc. of the American Control Conference (ACC)*, pp. 4661-4666, June 2012.

[19] A. Zulu and S. John, "A review of control algorithms for autonomous quadrotors," *Open Journal of Applied Sciences*, vol. 4, pp. 547-556, December 2014.

[20] N. S. Özbek, M. Önkol, and M. Ö. Efe, "Feedback control strategies for quadrotor-type aerial robots: A survey," *Transactions of the Institute of Measurement and Control*, vol. 38, pp. 529-554, October 2015.

[21] A. Kusalewicz, K. Armiński, and T. Zubowicz, "Użytkowy model matematyczny quadrocoptera do celów sterowania," *Zeszyty Naukowe Wydziału Elektrotechniki i Automatyki Politechniki Gdańskiej*, vol. 51, pp. 103-105, 2016. Zastosowanie komputerów w nauce i technice (In Polish).

[22] R. W. Beard and T. W. McLain, *Small Unmanned Aircraft: Theory and Practice*, Princeton University Press, Princeton, NJ, USA, 2012.

[23] N. S. Nise, *Control Systems Engineering*, 3rd ed., John Wiley & Sons, Inc., New York, NY, USA, 2000.

Tomasz Zubowicz received his M.Sc. Eng. degree in Control Engineering from the Faculty of Electrical and Control Engineering at the Gdańsk University of Technology in 2008. He received his Ph.D. Eng. (with honours) in the field of Control Engineering from the same faculty in 2019. In 2012, he became a permanent staff member at the Department of Control Systems Engineering at Gdansk University of Technology and a member of the IFAC T.C. 5.4 Large Scale Complex Systems. His current research interests concern the fuzzy control, model predictive control, biologically inspired control structures, monitoring, control and security of critical infrastructure systems.

Krzysztof Armiński received his M.Sc. Eng. degree in Control Engineering in 2009 from the Faculty Electrical and Control Engineering Department at the Gdańsk University of Technology. He received his Ph.D. Eng. (with honours) in the field of control engineering from the same faculty in 2014. Currently, he holds position of an assistant professor at the Department of Control Engineering, Gdansk University of Technology. His research interests include mathematical modelling and interval state estimation.

Arkadiusz Kusalewicz received his B.Sc. degree in Control Engineering in 2017 from Electrical and Control Engineering Department at Gdańsk University of Technology.